Acta Mechanica Sinica (2014) 30(5):727–738
DOI 10.1007/s10409-014-0064-3

RESEARCH PAPER

Stability and oscillations in a slow-fast flexible joint system with transformation delay

Shan-Ying Jiang · Jian Xu · Yao Yan

Received: 4 January 2014 / Revised: 19 March 2014 / Accepted: 17 April 2014

Abstract Flexible joints are usually used to transfer velocities in robot systems and may lead to delays in motion transformation due to joint flexibility. In this paper, a link-rotor structure connected by a flexible joint or shaft is firstly modeled to be a slow-fast delayed system when moment of inertia of the lightweight link is far less than that of the heavy rotor. To analyze the stability and oscillations of the slow-fast system, the geometric singular perturbation method is extended, with both slow and fast manifolds expressed analytically. The stability of the slow manifold is investigated and critical boundaries are obtained to divide the stable and the unstable regions. To study effects of the transformation delay on the stability and oscillations of the link, two quantitatively different driving forces derived from the negative feedback of the link are considered. The results show that one of these two typical driving forces may drive the link to exhibit a stable state and the other kind of driving force may induce a relaxation oscillation for a very small delay. However, the link loses stability and undergoes regular periodic and bursting oscillation when the transformation delay is large. Basically, a very small delay does not affect the stability of the slow manifold but a large delay affects substantially.

Keywords Flexible joint · Slow-fast system · Transformation delay · Geometric singular perturbation

1 Introduction

Systems composed of two or more coupled subsystems of different time scales are usually named as slow-fast systems [1], due to the coexistence of fast state variables and slow state variables in one system. In fact, some common coupled systems could be typical slow-fast systems under certain conditions, such as semiconductor lasers [2], predator-prey models [3], reaction-diffusion systems [4], etc. Generally, the difference of time scales comes from not only the slow-fast effects in real time, but also the scale effects in geometric size [5]. The rigid-link flexible-joint robot manipulator concerned in this paper is precisely such a slow-fast system when moment of inertia of the lightweight link (or arm) is far less than that of the heavy rotor, owing to the requirements of miniaturization and lightweight design.

In an early stage, robot manipulators were usually treated as rigid links connected by rigid actuated joints, though industrial applications had revealed the limitations of the rigid assumptions in modeling complicated dynamics. To gain a more accurate model, Spong [6] took the joint elasticity into consideration and proposed a mathematical model with flexible joints in 1980s. In his model, the reciprocal of the joint stiffness was introduced as a small parameter to separate different time scales. Moreover, as the limit of the joint stiffness tended to infinity, the flexible joint model degenerated into a rigid model, which verified the reasonableness of its modeling assumption. Extensive literatures on Spong's model mostly exist in the field of robot automation and control, dealing with position and control problems such as designs of different controllers, robust stability analyses and experimental investigations, etc. [7–12]. A detailed survey on the dynamic analyses of flexible robot manipulators was presented in Ref. [13].

The present study is motivated by the fact that there exists a so-called "transformation delay" in the motions of a flexible-joint. It is well known that the delay may induce instability. Starting from such views, many scholars reconsidered new control stage. Chen et al. [14, 15] introduced the time delay to improve Spong's model and consid-

The project was supported by the National Natural Science Foundation of China (11032009 and 11272236).

S.-Y. Jiang · J. Xu (✉) · Y. Yan
School of Aerospace Engineering and Applied Mechanics,
Tongji University, 200092 Shanghai, China
e-mail: xujian@tongji.edu.cn

ered the effects of flexible joints. The main interests were on the problem of controlling robot manipulators for trajectory tracking. Other works discussing the time delay influence were mainly based on Spong's original model and paid close attention to the time delays in feedback control. For example, in Ref. [16], the stability problem of a flexible-joint robot with time delays in the feedback loop was investigated. Meanwhile, an estimate of the system rate of convergence and a procedure for evaluating the region of attraction were presented. However, although there have been quite a number of contributions dealing with the delay effects, the transformation delay of motions was not taken into account. As a matter of fact, the flexibility of a joint or shaft may lead to a phase difference between two connected parts [17]. A key issue for our study is to treat the effect of this phase difference as a transformation delay in transferring the angular displacement from one side of the shaft to the other. Now that many studies have revealed that this delay may have a substantial effect on a dynamical system, it is desirable to make clear the influence of the transformation delay on the dynamics of slow-fast systems. Motivated by such issues, we remodel the rigid-link flexible-joint system and make a detailed discussion on the effects of transformation delay in the present paper.

According to the theory of nonlinear dynamics, systems with multiple time scales can exhibit complicated behaviors, such as relaxation oscillation [18], bursting [19], and spiking [20]. Nevertheless, regular perturbation methods [21] usually fail in analyzing these complex oscillations. To address the problem, a geometric approach named geometric singular perturbation method was initially proposed by Tikhonov [22] and Fenichel [23]. Furthermore, Jones [24] proved Fenichel's invariant manifold theorems and proposed the exchange lemma. The essence of this approach is to reformulate the singularly perturbed system into a fast system and a slow system with a transformation of time scales. Mathematically, limit of the fast system determines a set where the flow is trivial while limit of the slow system indicates a non-trivial flow on this set [24]. These two aspects are realized simultaneously in the geometric singular perturbation method. In the past several years, the idea of analyzing a slow-fast system from the geometric view has widely aroused interests in various fields. Rinaldi and Scheffer [25] discussed the interaction of the fast and slow processes that sometimes occurred in ecosystems. It was concluded that the geometric approach was very efficient in analyzing dynamic systems with up to three state variables, one of which was a slow variable. Meanwhile, this method vividly presented the mechanisms of sudden, surprising jumps of the ecological variables. A comprehensive description of spiking and bursting oscillations was accomplished by Izhikevich [26]. In his work, mechanisms of spiking and bursting were reviewed and the existing classification of various types of bursting was extended with application of the geometric bifurcation theory. After that, a hyperchaotic Lorenz system with two time scales was constructed by Han et al. [27]. Two types of bursting, symmetric fold/fold bursting, and symmetric sub-Hopf/sub-Hopf bursting were observed in their work. It is noticed that although the geometric singular perturbation method has been proven successful in analyzing a slow-fast system, limited work has been done in the analysis of a slow-fast system with time delay. One effort is made by Zheng and Wang [19]. They adopted the geometric singular perturbation method and revealed the time-delay effects on the bursting of the synchronized state of coupled Hindmarsh–Rose neurons. The stability analysis clarified the time-delay influence on the structure of the slow manifold, and then the transitions from bursting to relaxation oscillation and to chaotic bursting were investigated as well. Nevertheless, they did not mention the effect of the fast manifold, which is emphasized in our paper and seems to be another interesting issue.

The rest of this paper is organized as follows. In Sect. 2, a rigid-link flexible-joint robot arm is remodeled by taking the transformation delay into account, and then the singular perturbation technique is extended to analyze the delayed slow-fast system. Afterwards, Sect. 3 displays some interesting delay-induced oscillations by referring to the analytical results obtained in Sect. 2. The mechanisms of relaxation and bursting behaviors are analyzed in Sect. 4, followed by conclusions and extensions in Sect. 5.

2 Modeling and critical stability

Robot manipulators are usually designed as several rigid bodies connected by actuated joints. Traditional joints are treated as rigid connections, transferring the displacement as well as the velocity from one rigid body to another. However, the rigid assumption of the joints usually conflicts with industrial reality, where the joints are desired to be capable of bearing some axial clearance. As a result, engineering experience and intuition imply that the joints are more reasonable to be flexible. The mathematical model of a robot manipulator with flexibility was proposed by Spong in 1980s [6].

As we have stated in the previous section, the flexibility of a joint or a shaft may lead to a phase difference between two connected parts [17]. An ingenious idea is to treat the phase difference as a time delay, which is induced by transferring the angular displacement from one side of the shaft to another side. This time delay is called transformation delay and is actually the time of stress wave propagation along the shaft. In the following discussion, based on the contribution of Spong [6] and Chen and Shieh [14], we consider the effect of transformation delay originating from the couple of two components in one system.

2.1 Rigid-link flexible-joint model

In the rigid-link flexible-joint system [28], the rotor and the link are connected by a long elastic shaft, which is modeled as a liner torsion spring with stiffness K. As shown in Fig. 1, denote the moment of inertia of the link and the rotor as I and J, the angular displacement of the link and the rotor as

$\theta_1(t)$ and $\theta_2(t)$, respectively. Supposing that the angular displacement of the rotor at t_1 moment is transferred through the elastic shaft and arrives at the link at moment t_2 in the form of stress wave, one regards the transformation delay τ as time difference $t_2 - t_1$. Thus, the rigid-link flexible-joint robot manipulator system is remodeled, with the transformation delay in propagation or reaction process of two angular displacements taken into account, and the governing equation is given by

$$\begin{aligned} &I\ddot{\theta}_1(t) - c_1(\dot{\theta}_2(t) - \dot{\theta}_1(t-\tau)) - K(\theta_2(t) - \theta_1(t-\tau)) \\ &\quad + MgL\sin\theta_1(t) = 0, \\ &J\ddot{\theta}_2(t) + c_1(\dot{\theta}_2(t) - \dot{\theta}_1(t-\tau)) + K(\theta_2(t) - \theta_1(t-\tau)) \\ &\quad + c_2\dot{\theta}_2(t) = u(t), \end{aligned} \tag{1}$$

where $(\dot{}) = \mathrm{d}/\mathrm{d}t$ and $(\ddot{}) = \mathrm{d}^2/\mathrm{d}t^2$, M is the total mass of the link, L is the distance from the axis of rotation to the mass centre of the link, g is the acceleration constant of gravity and $u(t)$ the controlled torque to the shaft. c_1 and c_2 are the damping coefficients. With ignorance of the damping effects and the time delay, Eq. (1) degenerates into Spong's model [6, 28], which verifies our improvements. Detailed derivation of Spong's original model can be found in Ref. [6].

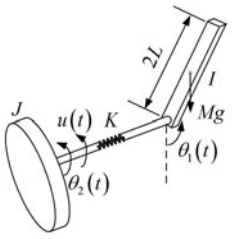

Fig. 1 The rigid-link flexible-joint robot manipulator, where the rotor is connected with the rigid link via an elastic long shaft modeled as a liner torsion spring with stiffness K

Normally, to move potentially heavy link, the rotor is designed to be very heavy. However, the weight of the link is variable, which can be very light in some situations. In these cases, it is uneasy to control the system when $I \ll J$ [29, 30]. We here consider a robot manipulator where an iron rotor of radius 250 mm and thickness 60 mm is connected with a lightweight cuboid link of length 250 mm, width 100 mm and thickness 40 mm via an elastic shaft with a length of 1 000 mm and a diameter of 3.5 mm. Thus, the parameters in Eq. (1) can be determined as

$$\begin{aligned} &I = 0.055\,\mathrm{kg}\cdot\mathrm{m}^2, \quad J = 2.897\,\mathrm{kg}\cdot\mathrm{m}^2, \\ &M = 2.65\,\mathrm{kg}, \quad g = 9.8\,\mathrm{ms}^2, \\ &K = 1.177\,99\,\mathrm{N}\cdot\mathrm{m}, \end{aligned} \tag{2}$$

where K is the equivalent torsional stiffness of the shaft.

To distinguish different scales, we introduce the following dimensionless parameters

$$\eta = \frac{I}{J}, \quad \alpha_1 = \frac{c_1}{\sqrt{KJ}}, \quad \alpha_2 = \frac{c_2}{\sqrt{KJ}}, \quad \beta = \frac{MgL}{K}. \tag{3}$$

Substituting Eq. (3) into Eq. (1) yields

$$\begin{aligned} &\eta\ddot{\theta}_1(t) - \alpha_1(\dot{\theta}_2(t) - \dot{\theta}_1(t-\tau)) \\ &\quad -(\theta_2(t) - \theta_1(t-\tau)) + \beta\sin\theta_1(t) = 0, \\ &\ddot{\theta}_2(t) + \alpha_1(\dot{\theta}_2(t) - \dot{\theta}_1(t-\tau)) \\ &\quad +(\theta_2(t) - \theta_1(t-\tau)) + \alpha_2\dot{\theta}_2(t) = u(t). \end{aligned} \tag{4}$$

Considering Eqs. (2) and (3), we have $\eta \sim 10^{-2}$, $\alpha_1 \sim 10^{-1}$, $\beta \sim 10^0$, $\alpha_2 \sim 10^1$. Letting $\eta = \varepsilon^2$, $0 < \varepsilon \ll 1$ and $\alpha_1 = \varepsilon\bar{\alpha}_1$ yields that Eq. (4) becomes a typical slow-fast system with delay coupling, which is

$$\begin{aligned} &\varepsilon\dot{\theta}_1(t) = p_1(t), \\ &\varepsilon\dot{p}_1(t) = \bar{\alpha}_1(\varepsilon p_2(t) - p_1(t-\tau)) \\ &\quad +(\theta_2(t) - \theta_1(t-\tau)) - \beta\sin\theta_1(t), \\ &\dot{\theta}_2(t) = p_2(t), \\ &\dot{p}_2(t) = -\bar{\alpha}_1(\varepsilon p_2(t) - p_1(t-\tau)) \\ &\quad -(\theta_2(t) - \theta_1(t-\tau)) - \alpha_2 p_2(t) + u(t). \end{aligned} \tag{5}$$

It is obtained from Eq. (5) that a small parameter ε multiplies the highest derivative of the state variables, which leads to the singularity. Actually, the singularity comes from the fact that the order of the system for $\varepsilon = 0$ becomes lower than that for $\varepsilon \neq 0$. Such systems are also called singular perturbation systems [31].

2.2 Geometric singular perturbation analysis

We now turn to the problem of geometric singular perturbation analysis of the slow-fast system with delay coupling. Our basic equations are of the form of as

$$\begin{aligned} &\varepsilon\dot{x}(t) = f(x(t), y(t), x(t-\tau), y(t-\tau), \varepsilon), \\ &\dot{y}(t) = g(x(t), y(t), x(t-\tau), y(t-\tau), \varepsilon), \end{aligned} \tag{6}$$

where $x \in \mathbb{R}^n$, $y \in \mathbb{R}^l$, τ is a real parameter and $0 < \varepsilon \ll 1$.

Reformulating system (6) with a change of time-scale $t = \varepsilon\bar{t}$ and denoting $x(\varepsilon\bar{t})$, $y(\varepsilon\bar{t})$ as $x(\bar{t})$, $y(\bar{t})$ yields

$$\begin{aligned} &x'(\bar{t}) = f(x(\bar{t}), y(\bar{t}), x(\bar{t}-\bar{\tau}), y(\bar{t}-\bar{\tau}), \varepsilon), \\ &y'(\bar{t}) = \varepsilon g(x(\bar{t}), y(\bar{t}), x(\bar{t}-\bar{\tau}), y(\bar{t}-\bar{\tau}), \varepsilon), \end{aligned} \tag{7}$$

where $(') = \mathrm{d}/\mathrm{d}\bar{t}$. It is obvious that these two systems are equivalent as long as $\varepsilon \neq 0$. Moreover, system (7) is called the fast system whereas system (6) the slow system, for the fact that the time scale given by $\bar{t}$ is faster than that for t while $t = \varepsilon\bar{t}$ and $0 < \varepsilon \ll 1$. As $\varepsilon \to 0$, a reduced fast subsystem

$$\begin{aligned} &x'(\bar{t}) = f(x(\bar{t}), y(\bar{t}), x(\bar{t}-\bar{\tau}), y(\bar{t}-\bar{\tau}), 0), \\ &y'(\bar{t}) = 0, \end{aligned} \tag{8}$$

and a reduced slow subsystem

$$
\begin{aligned}
&f(x(t), y(t), x(t-\tau), y(t-\tau), 0) = 0,\\
&\dot{y}(t) = g(x(t), y(t), x(t-\tau), y(t-\tau), 0),
\end{aligned}
\tag{9}
$$

are obtained. Defining the equilibrium condition of subsystem (8) as the slow manifold M_0 and that of subsystem (9) as the fast manifold M_ε, the geometric singular perturbation theory [22–24] guarantees that the dynamics of the original system (6) can be approximated by the behaviors of the reduced fast subsystem (8) on the slow manifold M_0. On the other hand, the invariant manifold M_ε could be considered as a small perturbation to M_0. Therefore, a crucial step in the process of geometric singular perturbation analysis is to identify the structure as well as the stability of the slow manifold M_0. After that, taking the effect of the fast manifold M_ε into consideration helps to determine the flows of the full system in the phase space.

Proceeding as in the previous paragraph, we rescale system (5) by $t = \varepsilon\bar{t}$. Thus, as $\varepsilon \to 0$, the reduced fast subsystem is

$$
\begin{aligned}
&\theta_1'(\bar{t}) = p_1(\bar{t}),\\
&p_1'(\bar{t}) = -\bar{\alpha}_1 p_1(\bar{t}-\bar{\tau}) + (\theta_2(\bar{t}) - \theta_1(\bar{t}-\bar{\tau})) - \beta\sin\theta_1(\bar{t}),\\
&\theta_2'(\bar{t}) = 0,\\
&p_2'(\bar{t}) = 0.
\end{aligned}
\tag{10}
$$

In the following discussion, $\bar{t}$ and $\bar{\tau}$ are still denoted as t and τ for convenience.

It follows from the geometric singular perturbation theory that the dynamics of system (5) is determined by the structure and the stability of the slow manifold. Specifically, the slow manifold of Eq. (5) is the equilibrium of the fast subsystem (10). Since the delay does not affect the equilibrium, it follows from Eq. (10) that the slow manifold is represented by

$$
\begin{aligned}
M_0 = \{&(\theta_1, p_1, \theta_2, p_2) \in \mathrm{R}^4 : p_1(t) = 0,\\
&-\bar{\alpha}_1 p_1(t) + (\theta_2(t) - \theta_1(t)) - \beta\sin\theta_1(t) = 0\}.
\end{aligned}
\tag{11}
$$

It is well known that the delay may have a substantial effect on the stability of the equilibrium solutions [32, 33]. Therefore, it is necessary to display the relation between the delay and the stability of the slow manifold obtained in Eq. (11). To this end, we investigate the characteristic equation of the fast subsystem (10), which is

$$
D(\lambda) = \lambda^2 + \mathrm{e}^{-\lambda\tau}\bar{\alpha}_1\lambda + \mathrm{e}^{-\lambda\tau} + \beta\cos\theta_1 = 0. \tag{12}
$$

Based on the stability theory, a stable slow manifold requires that all the eigenvalues should have negative real parts. In other words, when any of the eigenvalues has a positive real part, the slow manifold loses its stability. It implies that the critical situations for Eq. (12) is $\lambda = 0$ or $\lambda = \pm\mathrm{i}\omega$ ($\omega > 0$). It is easy to see that for $1 + \beta\cos\theta_1 = 0$, $\lambda = 0$ is a root of Eq. (12), while $1 + \beta\cos\theta_1 \neq 0$ gives $\lambda \neq 0$. However, in the case of $1 + \beta\cos\theta_1 \neq 0$, Eq. (12) can still propose a pair of pure imaginary roots $\lambda = \pm\mathrm{i}\omega$ ($\omega > 0$). Substituting it into Eq. (12) and separating the real and the imaginary parts, one has

$$
\begin{aligned}
&-\omega^2 + \beta\cos\theta_1 + \cos(\omega\tau) + \bar{\alpha}_1\omega\sin(\omega\tau) = 0,\\
&\bar{\alpha}_1\omega\cos(\omega\tau) - \sin(\omega\tau) = 0.
\end{aligned}
\tag{13}
$$

Rearranging Eq. (13) yields that

$$
\begin{aligned}
\sin(\omega\tau) &= \frac{\bar{\alpha}_1\omega(\omega^2 - \beta\cos\theta_1)}{1 + \bar{\alpha}_1^2\omega^2},\\
\cos(\omega\tau) &= \frac{\omega^2 - \beta\cos\theta_1}{1 + \bar{\alpha}_1^2\omega^2}.
\end{aligned}
\tag{14}
$$

To solve Eq. (14), we can use trigonometric identity $\sin^2(\omega\tau) + \cos^2(\omega\tau) \equiv 1$ to construct a function

$$
\begin{aligned}
F(\Omega) &= \sin^2(\omega\tau) + \cos^2(\omega\tau) - 1\\
&= \frac{1}{1 + \bar{\alpha}_1^2\Omega}[\Omega^2 - (\bar{\alpha}_1^2 + 2\beta\cos\theta_1)\Omega\\
&\quad + \beta^2\cos^2\theta_1 - 1],
\end{aligned}
\tag{15}
$$

where $\Omega = \omega^2$. When Eq. (14) do have real solutions, the equality $F(\Omega) = 0$ holds. Otherwise, $F(\Omega) \neq 0$. Therefore, the critical eigenvalues (pure imaginary eigenvalues) determining the stability of the slow manifold can be solved by Eq. (15). For example, one may have $\bar{\alpha}_1 = 1$, $\beta = 3$ if the system is designed with the parameters given by Eq. (2). Then it is easy to obtain the critical eigenvalues by solving $F(\Omega) = 0$, which are shown in Fig. 2.

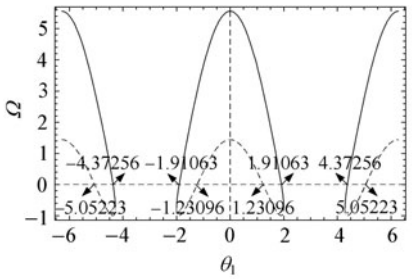

Fig. 2 The roots of $F(\Omega) = 0$ on the plane Ω–θ_1 with $\theta_1 \in [-2\pi, 2\pi]$, where the solid curves denote one root and the dashed curves denote another one. Since $\Omega = \omega^2(\omega > 0)$, only positive roots $\Omega > 0$ are meaningful

All the curves in Fig. 2 illustrate $F(\Omega) = 0$. However, only the curves with positive Ω is meaningful since $\Omega = \omega^2(\omega > 0)$. Therefore, it is obtained from Fig. 2 that when $\theta_1 \in [0, 1.230\,96)$ and $\theta_1 \in (5.052\,23, 2\pi]$, there are two solutions, $\omega_1 = \sqrt{\frac{1}{2}(1 + 6\cos\theta_1 - \sqrt{5 + 12\cos\theta_1})}$ and $\omega_2 = \sqrt{\frac{1}{2}(1 + 6\cos\theta_1 + \sqrt{5 + 12\cos\theta_1})}$, meeting the requirements. On the other hand, there is only one solution, $\omega_2 = \sqrt{\frac{1}{2}(1 + 6\cos\theta_1 + \sqrt{5 + 12\cos\theta_1})}$ in the interval of $(1.230\,96, 1.910\,63)$ and $(4.372\,56, 5.052\,23)$. In the case of $\theta_1 \in (1.910\,63, 4.372\,56)$, however, there is no solution.

Without loss of generality, the following analysis is located in $\theta_1 \in [0, 2\pi]$ since Eq. (15) is periodic with respect to θ_1.

After eigenvalues are obtained, the relationship between τ and θ_1 is to be discussed. To begin with, when $\Omega = 0$, one has $\lambda = 0$, corresponding to the intersection. points when $\theta_1 = 1.910\,63$ and $\theta_1 = 4.372\,56$ in Fig. 2. To figure out the evaluation of the zero eigenvalue as θ_1 crossing the above critical values, the following expression is obtained from Eq. (12)

$$\frac{\mathrm{d}}{\mathrm{d}\theta_1}\lambda(\theta_1) = \frac{\beta \sin\theta_1}{2\lambda - \tau \mathrm{e}^{-\lambda\tau}\bar{\alpha}_1\lambda + \mathrm{e}^{-\lambda\tau}\bar{\alpha}_1 - \tau\mathrm{e}^{-\lambda\tau}}. \tag{16}$$

Substituting $\lambda = 0$ into Eq. (16), one gains

$$\begin{aligned}&\Re\Big(\frac{\mathrm{d}}{\mathrm{d}\theta_1}\lambda(\theta_1)\Big|_{\theta_1=1.910\,63}\Big)\\ &= \Re\Big(\frac{\beta\sin\theta_1}{\bar{\alpha}_1 - \tau}\Big|_{\theta_1=1.910\,63}\Big)\begin{cases} > 0, & \tau < \bar{\alpha}_1,\\ < 0, & \tau > \bar{\alpha}_1,\end{cases}\end{aligned} \tag{17}$$

and

$$\begin{aligned}&\Re\Big(\frac{\mathrm{d}}{\mathrm{d}\theta_1}\lambda(\theta_1)\Big|_{\theta_1=4.372\,56}\Big)\\ &= \Re\Big(\frac{\beta\sin\theta_1}{\bar{\alpha}_1 - \tau}\Big|_{\theta_1=4.372\,56}\Big)\begin{cases} > 0, & \tau < \bar{\alpha}_1,\\ < 0, & \tau > \bar{\alpha}_1,\end{cases}\end{aligned} \tag{18}$$

where $\Re(r)$ represents the real part of the expression.

According to Eqs. (17) and (18), we may summarize that the real part of the eigenvalue $\lambda = 0$ increases with θ_1 crossing $\theta_1 = 1.910\,63$ and decreases with θ_1 crossing $\theta_1 = 4.372\,56$ when $\tau < \bar{\alpha}_1$. Thus, lines $\theta_1 = 1.910\,63$ and $\theta_1 = 4.372\,56$ indicate two critical boundaries of fold bifurcation underneath the horizontal line $\tau = \bar{\alpha}_1$.

When $\Omega > 0$, substituting ω_1 and ω_2 into Eq. (14) yields

$$\begin{aligned}&\tau_1 = \frac{1}{\omega_1}\Big\{2m\pi + \pi - \arcsin\Big[\frac{\omega_1(\omega_1^2 - 3\cos\theta_1)}{1+\omega_1^2}\Big]\Big\},\\ &\qquad m = 0, 1, 2, \cdots,\\ &\tau_2 = \frac{1}{\omega_2}\Big\{2n\pi + \arcsin\Big[\frac{\omega_2(\omega_2^2 - 3\cos\theta_1)}{1+\omega_2^2}\Big]\Big\},\\ &\qquad n = 0, 1, 2, \cdots.\end{aligned} \tag{19}$$

Figure 3 shows the corresponding boundaries on plane $\tau - \theta_1$, where the dashed lines are critical boundaries formulated in τ_1 expression, the solid lines in τ_2 expression and the dash-dot lines are boundaries obtained when $\lambda = 0$.

Before proceeding further, let us take a look on the magnitude of the transformation delay in engineering applications. As mentioned earlier, the transformation delay is considered as the propagation time of stress wave along the elastic shaft. Without loss of generality, two kinds of common materials, i.e., a steel shaft and a rubber shaft are taken into consideration. Since the length of the shaft is 1 000 mm, the propagation velocity of elastic torsion wave in steel is

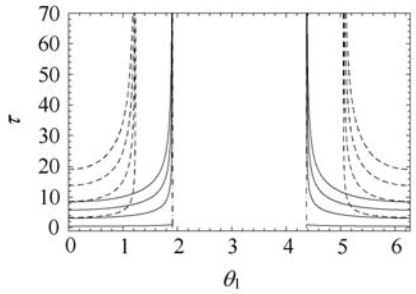

Fig. 3 Critical boundaries on plane τ–θ_1, where the dashed lines are the critical boundaries formulated in τ_1, the solid lines in τ_2 and the dash-dot boundaries are obtained when $\lambda = 0$

3.22 km/s [34], and that in rubber is 0.027 km/s [34], dividing the length of the shaft by the propagation velocity yields that the propagation time is 0.000 310 559 s in steel shaft and 0.037 037 s in rubber shaft. With the same method, the propagation time in other common materials such as aluminum and copper can be obtained. It turns out that a reasonable value of the transformation delay would be limited in the interval of (0.000 310 559 s, 0.037 037 s) in the considered system. In fact, a large transformation delay has no physical meaning since it does not exist in real engineering.

As mentioned above, the slow manifold determines the dynamical behaviors of the system under consideration. Therefore, it is necessary to discuss the effects of time delays on the stability of the slow manifold. Meanwhile, considering the time scale transformation of $t = \varepsilon\bar{t}$ in Eq. (10), the meaningful value of the time delay would be limited within $0 \leqslant \tau \leqslant 10^{-1}$ when $\varepsilon = 0.1$. In the next section, to get a full picture of the time-delay influence, we will discuss five cases within $0 \leqslant \tau \leqslant 5$ at first, and then in Sect. 4, those cases satisfying physical reality will be displayed.

3 Stability of slow manifold

In this section, we analyze the stability of the slow manifold (11) in various regions shown in Fig. 4, which is actually a zoom of Fig. 3. It follows from Fig. 4 that the critical boundaries separate the plane $P = \{(\theta_1, \tau) : 0 \leqslant \theta_1 \leqslant 2\pi, 0 \leqslant \tau \leqslant 5\}$ into nine regions, denoted as I, II, III, IV, I′, II′, III′, IV′,

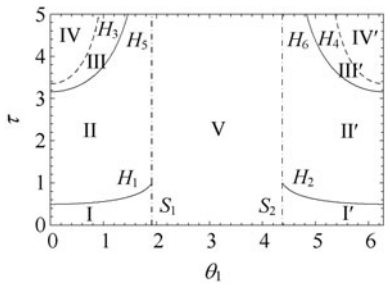

Fig. 4 Various regions divided by the critical boundaries, where the dash-dot boundaries are labeled in S_1 and S_2, the solid in H_1, H_2, H_5, H_6, and the dashed in H_3 and H_4 for $\bar{\alpha}_1 = 1, \beta = 3$

and V. The stability of the slow manifold may be distinct in these regions. We only analyze that in Regions I, II, III, IV, and V due to symmetry when $0 \leqslant \theta_1 \leqslant 2\pi$.

To study the stability in each region, the Argand diagram is used to observe evolution of the eigenvalues. To illustrate, we let $\theta_1 = 0.4$ and τ changing from 0 to 5, as the dashed line shown in Fig. 5a. It should be noted that the delay induces infinite eigenvalues of Eq. (12). Only the right-most two conjugate pairs of eigenvalues are presented in Fig. 5b. It is seen that the conjugate pairs remain having negative real parts until τ reaches the boundary labeled H_1 (see Fig. 4). With τ crossing H_1 or varying from Region I to II, the real parts of the minimum-mode conjugate pair become positive and the other pair still has negative real parts. It is also seen from Fig. 5 that another conjugate pair passes through the imaginary axis with τ varying from Region II to III. In Region IV, however, the real parts of a pair of conjugate eigenvalues return negative after crossing the boundary labeled H_3. Referring to Refs. [32, 33], one may know that the Hopf bifurcation occurs in the boundary labeled H_1. Thus, we can summarize the above analysis, that is, the slow manifold is stable in Region I but loses its stability in Region II, and it goes more unstable in Region III but less stable in Region IV. It should be noted that the delay does not affect the stability of the slow manifold when θ_1 is located in Region V. Therefore, the stability in Region V for any delay is the same as that for $\tau = 0$. Similarly, the slow manifold is stable in Region I′ and unstable in II′, III′, and IV′ due to symmetry.

After the stability is clarified, Fig. 5 can be used to predict the potential joint motions in realistic applications. To demonstrate, five typical cases are selected. Corresponding to five fixed values of delay, we choose

(1) Case 1 for the delay when θ_1 crosses through Regions I, V, and I′,

(2) Case 2 for the delay θ_1 crossing through Regions II, I,V, I′, and II′,

(3) Case 3 for the delay θ_1 varying among Regions II, V, and II′,

(4) Case 4 for θ_1 varying among Regions III, II, V, II′, and III′,

(5) Case 5 for θ_1 through Regions IV, III, II, V, II′, III′, and IV′.

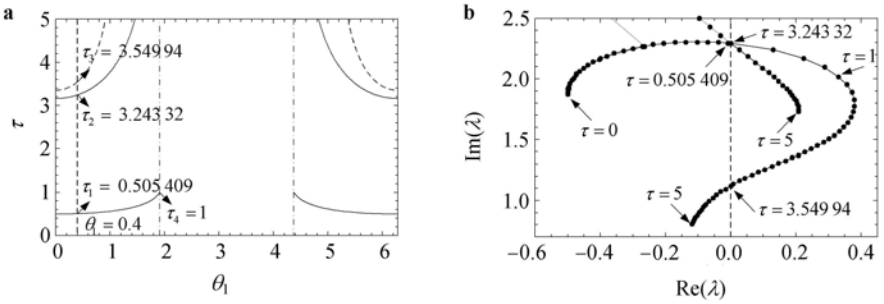

Fig. 5 Argand diagram of eigenvalues of Eq. (12) with τ varying from 0 to 5 for $\theta_1 = 0.4$, where **a** illustrates the critical boundaries and **b** is the corresponding Argand diagram

For Case 1, the slow manifold is stable when θ_1 is in Regions I and I′ but is unstable for θ_1 in Region V. For Case 2, the slow manifold is unstable initially for a small angular displacement of the arm or link θ_1 but becomes stable when θ_1 enters into Region I, and returns unstable afterwards. Clearly, no stable slow manifold is available for Cases 3, 4 or 5. The stability of the slow manifold for the above five cases are also shown in Fig. 6. In Fig. 6, the solid curves denote the stable segments of the slow manifold, while the dashed curves display the unstable segments, with H_i, S_i $(i = 1, 2, \cdots)$ illustrating the boundaries shown in Fig. 4.

Physically, it is hoped that the link or arm is stable when it is driven to a desired angular position. It follows from Fig. 6 that the link may lose stability for some angular positions, which is induced by the transformation delay. Besides the delay, the driving force may also play a very important role. Thus, it is necessary to design an appropriate driving force for a stable link motion. This is to be discussed in the next section.

4 Amplitude death and oscillations

To understand the relation between the system stability and the driving force $u(t)$ in Eq. (5), we employ the geometric singular perturbation method again by referring to the five cases shown in Fig. 6.

After the stability of fast subsystem is investigated in Sect. 3, the slow subsystem must be studied as well. It is easy to see that as $\varepsilon \to 0$, the reduced slow subsystem derived from Eq. (5) turns into

$$\begin{aligned} &p_1(t) = 0, \\ &-\bar{\alpha}_1 p_1(t-\tau) + (\theta_2(t) - \theta_1(t-\tau)) \\ &\qquad -\beta \sin\theta_1(t) = 0, \\ &\dot{\theta}_2(t) = p_2(t), \\ &\dot{p}_2(t) = \bar{\alpha}_1 p_1(t-\tau) - (\theta_2(t) - \theta_1(t-\tau)) \\ &\qquad -\alpha_2 p_2(t) + u(t). \end{aligned} \tag{20}$$

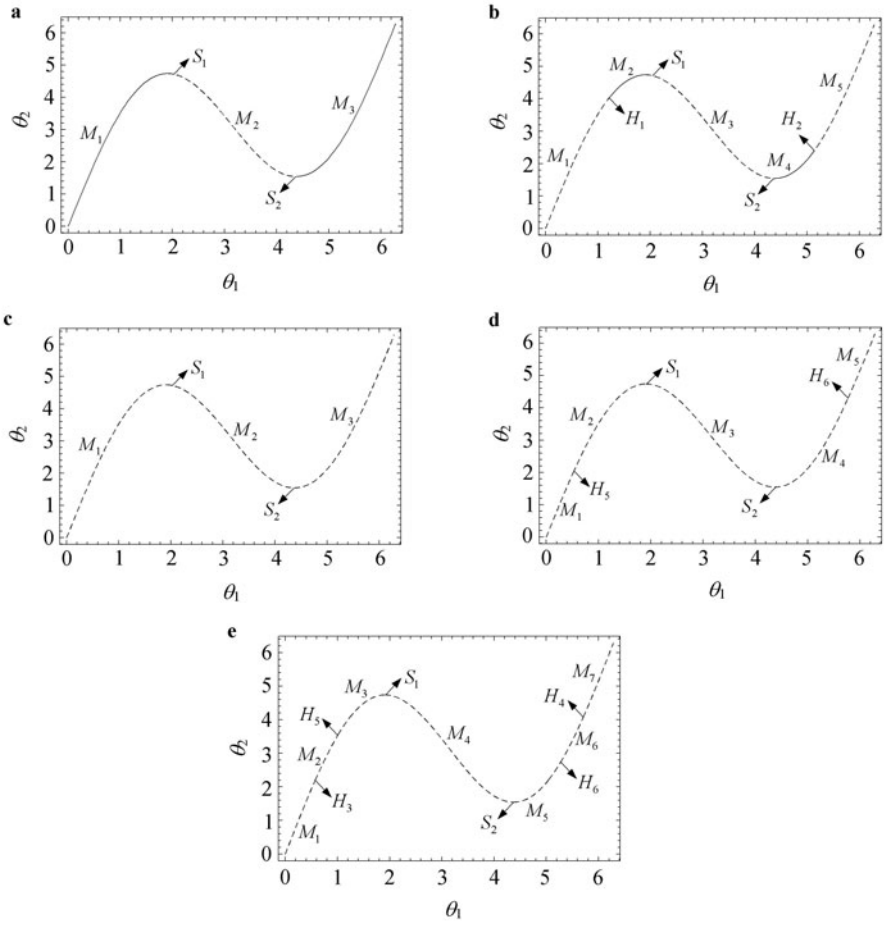

Fig. 6 Stability and structure of slow manifold (11) for **a** Case 1 , $\tau = 0.4$; **b** Case 2, $\tau = 0.6$; **c** Case 3, $\tau = 2$; **d** Case 4, $\tau = 3.3$; **e** Case 5, $\tau = 3.8$, where the solid curves denote the stable segments of the slow manifold, the dashed curves display the unstable segments and H_i, S_i correspond to the boundaries shown in Fig. 4

According to the definition of the fast manifold [24], one gains

$$M_\varepsilon = \{(\theta_1, p_1, \theta_2, p_2) \in \mathbb{R}^4 : p_2(t) = 0, \\ \bar{\alpha}_1 p_1(t-\tau) - (\theta_2(t) - \theta_1(t-\tau)) - \alpha_2 p_2(t) + u(t)\} = 0, \quad (21)$$

on which the driving force $u(t)$ affects.

To observe the angular displacement of the rotor and the arm, the fast manifold M_ε is projected onto plane θ_1–θ_2, leading to

$$\theta_2(t) = \theta_1(t-\tau) + u(t). \quad (22)$$

In practice, the arm is driven by the control force $u(t)$ to move to a desired position. To this end, a linear driving force, which is the simplest controller, can be used as follows

$$u(t) = a\theta_1(t) + b, \quad (23)$$

where a and b are constants, determining desired positions of the arm. With this control, the relations among the driving force, the fast manifold and the slow manifold can be observed. This is to be done by utilizing various geometric diagrams on plane θ_1–θ_2.

4.1 Effect of slow manifold

To the end mentioned above, starting from the case of $u(t) = 0$, namely $a = 0$ and $b = 0$, we first extend the geometric perturbation analysis to the slow-fast delayed system. Figure 7 shows the geometry of the fast and slow manifolds without driving force, corresponding to those five stability switch forms of the slow manifold that are displayed in Fig. 6, where the fast manifold is displayed by the dotted line M_ε.

It follows from Fig. 7a that there are three intersections of the slow and the fast manifolds, denoted as E_1, E_2, and E_3, respectively. These intersections are actually three equilibriums of the full system (5), according to the fact that the slow and the fast manifolds are null lines of the two subsystems of system (5). According to the theory of geometric perturbation, one can conclude that E_1 and E_3 are stable but E_2 is unstable. Thus, E_1 and E_3 are two attractors on plane θ_1–θ_2. Observing and analyzing the geometry in Fig. 7a, one can easily obtain the attraction basin of E_3 [35], as shown in the shaded zone of Fig. 7a. It can be concluded that the rest region is the attraction basin of E_1 due to symmetry. Such analytical conclusion leads to an implication that the link or arm

always keeps stable when it is subjected to a small external disturbing which is confirmed by the numerical simulation results shown in Fig. 8. Moreover, it means that the designed parameter is reasonable for Case 1 or a small transformation delay.

For Case 2 shown in Fig. 7b, the fast manifold intersects with the unstable branches of the slow manifold at three points, where E_2 is unstable and has the same behaviors as that in Case 1. However, E_1 and E_3 lose their stability and undergo a Hopf bifurcation [36, 37] into periodic motions or limit cycles. They become new attractors on plane θ_1–θ_2. It suggests that the flow starting from any given initial values on the θ_1–θ_2 plane moves in the direction of the arrows displayed in Fig. 7b and gradually towards one of the limit cycles, which is verified in Fig. 9. Namely, the attraction basin in Fig. 7a becomes that in Fig. 7b, being the attraction of periodic motions rather than that of equilibriums. Physically, the transformation delay begins to have a substantial effect on the system under consideration, resulting in periodic vibration with distinct phase for the link and the rotor.

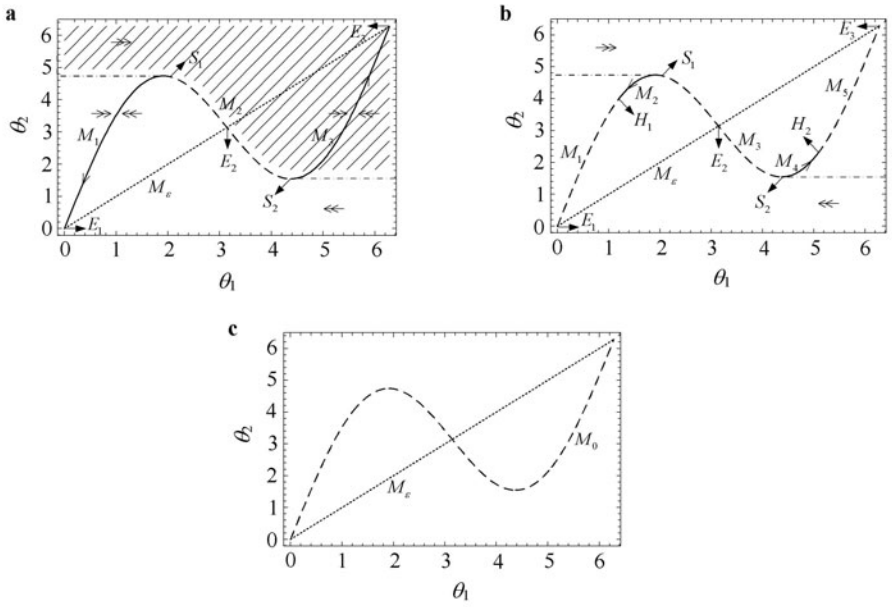

Fig. 7 Geometry of slow and fast manifolds on plane θ_1–θ_2 for **a** Case 1, $\tau = 0.4$; **b** Case 2, $\tau = 0.6$; **c** Case 3, $\tau = 2$; Case 4, $\tau = 3.3$; Case 5, $\tau = 3.8$ when $u(t) = 0$ and $\bar{\alpha}_1 = 1, \beta = 3, \alpha_2 = 10, \varepsilon = 0.1$

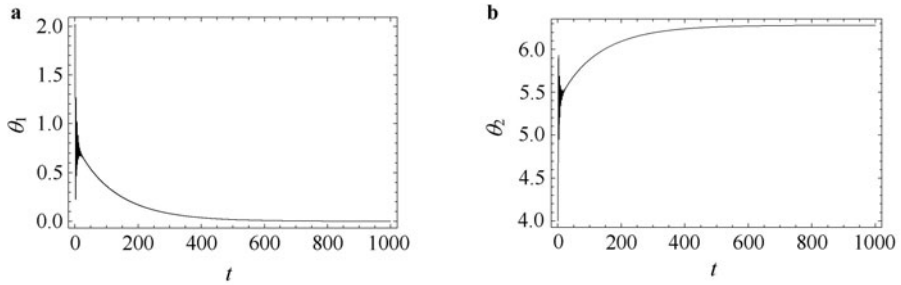

Fig. 8 Time histories of the stable link or arm for the initial values given by **a** $(\theta_1, \theta_2) = (2, 3)$ and **b** $(\theta_1, \theta_2) = (4, 3)$, respectively

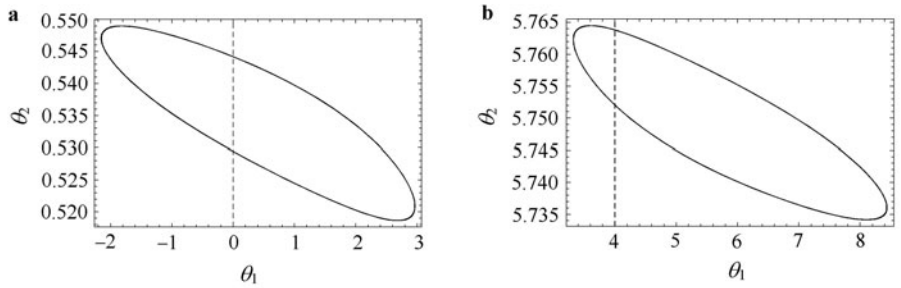

Fig. 9 Relation between the link θ_1 and the rotor θ_2 for Case 2, showing periodic vibration with distinct phase at the initial values given by **a** $(\theta_1, \theta_2) = (2, 3)$ and **b** $(\theta_1, \theta_2) = (4, 3)$, respectively

It follows from Fig. 7c that any convergent solutions of Eq. (5) can not be obtained for Case 3 or for a larger delay, which is also confirmed by the numerical simulation. It means that Case 3 loses its physical meaning. Therefore, we will not investigate this case any more in the following discussion.

4.2 Effect of fast manifold

Following the analysis in terms of geometric perturbation technique, we now return to the system subjected to a driving force given by Eq. (23) to study both Cases 1 and 2 displayed in Figs. 7a and 7b in a similar way.

Substituting Eq. (23) into Eq. (22) yields

$$\theta_2(t) = a\theta_1(t) + \theta_1(t-\tau) + b. \tag{24}$$

From Eq. (24), one can see that slope of the projection of the fast manifold on plane θ_1–θ_2 may be either positive or negative, which is determined by the coefficient a in the driving force (23). Thus, two typical driving forces presented in Eq. (23) will be discussed, i.e., $a > -1$ and $a < -1$, corresponding to the positive slope and the negative slope of the projection of the fast manifold (21). Figure 10 shows the geometry of the slow and the fast manifold on plane θ_1–θ_2 for $a > -1$. Comparing Fig. 10 with Fig. 7, one can see that geometry of the slow and the fast manifolds on plane θ_1–θ_2 is qualitatively identical. It implies that the dynamical features are the same as that of the case for $u(t) = 0$.

Another typical driving force is modeled for $a < -1$, and the intersection of the fast and the slow manifolds on plane θ_1–θ_2 is unique, as shown in Fig. 11. In Fig. 11, the unique intersection denoted as E_2 represents also the equilibrium of Eq. (5), and the double and the single arrows display the phase trajectories of the fast and the slow flows respectively. Figure 11a shows that there is no stable equilibrium on plane θ_1–θ_2 even for a small transformation delay. It means that the flow starting from any points on plane θ_1–θ_2 will be attracted by a stable slow manifold, either M_1 or M_2. For example, the flow starting from an initial point $(\theta_1, \theta_2) = (2, 3)$ is attracted by the stable manifold M_1 in a jogging way and then moves slowly along M_1 by S_1 at which a trivial eigenvalue appears. It yields that the flow is repelled so that it jumps to another stable branch M_3, shakes towards M_3 and moves slowly along M_3 by S_2 at which it is repelled. Then, such course is repeated again, resulting in a parallelogram-like limit cycle, as shown in Fig. 12. To understand the above analysis physically, we plot the time histories of the angular displacements of both the link and the rotor in Fig. 13. It follows from Figs. 11a, 12, and 13 that oscillations of the link and the rotor exhibit periodic bursting-like behaviors [38] with shaking. Such motions undergo two slow courses when the trajectory moves along the stable branches of the slow manifold and two fast courses when the trajectory jumps from one stable branch to another. Thus, it is well known that this kind of bursting-like oscillation is the so-called relaxation oscillation between the slow manifold and the fast manifold.

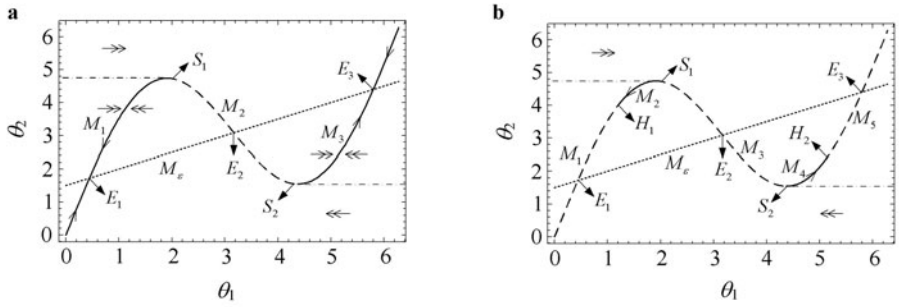

Fig. 10 Geometry of slow and fast manifolds on plane θ_1–θ_2 for **a** Case 1, $\tau = 0.4$; **b** Case 2, $\tau = 0.6$, when $u(t) = a\theta_1(t) + b$, $a = -0.5$, $b = 1.5$, and $\bar{\alpha}_1 = 1, \beta = 3, \alpha_2 = 10, \varepsilon = 0.1$

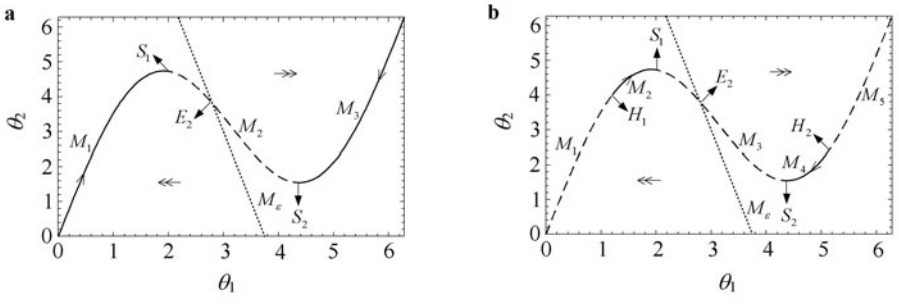

Fig. 11 Geometry of slow and fast manifolds on plane θ_1–θ_2 for **a** Case 1, $\tau = 0.4$; **b** Case 2, $\tau = 0.6$, when $u(t) = a\theta_1(t) + b$, $a = -5$, $b = 15$, and $\bar{\alpha}_1 = 1, \beta = 3, \alpha_2 = 10, \varepsilon = 0.1$

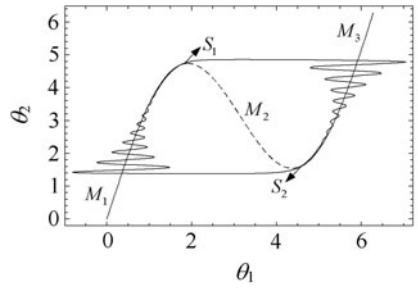

Fig. 12 Flow trajectory of Eq. (5) for Case 1 shown in Fig. 11a on plane θ_1–θ_2

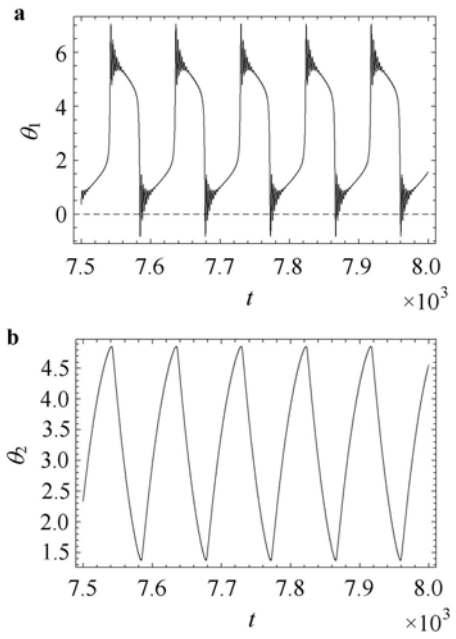

Fig. 13 Time histories of the angular displacements of both link and rotor in Eq. (5) for Case 1 shown in Fig. 11a, where **a** $\theta_1 - t$ and **b** $\theta_2 - t$

For a large transformation delay, i.e., Case 2 shown in Fig. 11b, when $a = -5$, $b = 15$, the fast manifold M_ε intersects with the unstable manifold M_3 at the equilibrium E_2, and thus there is no attractor on plane θ_1–θ_2. Compared with the structure of the slow manifold in Fig. 11a, the left and the right stable branches are shortened into two stable branches M_2 and M_4, losing stability at the Hopf points H_1, H_2 and arousing limit cycles centering at the unstable branches M_1 and M_5. As an example shown in Fig. 14, starting from an initial point $(\theta_1, \theta_2) = (2, 3)$, the solution trajectory is firstly attracted to the left limit cycle, as a fast process indicated by the double arrow. Then, it moves slowly around the limit cycle and shrinks to the Hopf point H_1, continues to move along the stable manifold M_2 until the first fold point S_1 is reached. Thereafter, it jumps horizontally to the right limit cycle, being attracted and shrinks slowly to the second Hopf point H_2. It sticks to the stable manifold M_4 until the second fold point S_2 is reached, continued by a fast jump to the left limit cycle, being attracted and forms a special limit cycle illustrated in Fig. 14. It is also confirmed by the time histories of the link and the rotor displayed in Fig. 15.

According to Fig. 14, the movement of the link exhibits a switch between two shrinking periodic oscillations centering at two different equilibrium positions. This kind of oscillation with periodic clusters is called bursting oscillation. Moreover, according to the bifurcation mechanism of this oscillation, it can be further classified as Hopf/Hopf bursting [5].

Now we give a brief summary to close this section. For two typical cases of transformation delay, we have considered two quantitatively different driving forces to investigate the stability and oscillations of the system under consideration. For the case of a small delay, both the link and the rotor exhibit a stable state under the first kind of driving force,

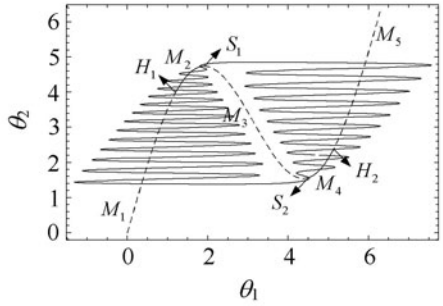

Fig. 14 Flow trajectory of Eq. (5) for Case 2 shown in Fig. 11b on plane θ_1–θ_2

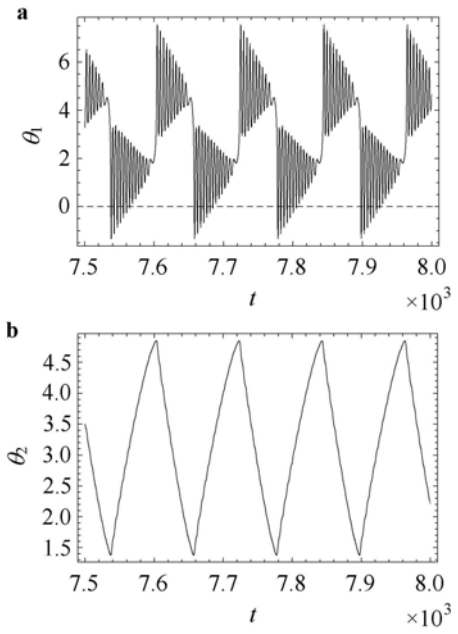

Fig. 15 Time histories of the angular displacements of both link and rotor in Eq. (5) for Case 2 shown in Fig. 11b, where **a** θ_1–t and **b** θ_2–t

whereas lose their stability to undergo a relaxation oscillation with shaking under the second kind. For the case of a large delay, two types of driving forces lead to a regular periodic oscillation at first and then such oscillation is enhanced to be a bursting, in which the instability of the system becomes worse. It implies that an appropriate design for both the flexible joint and the driving force is very important. Otherwise, one may observe more complicated oscillations of the system, such as different types of bursting and chaotic oscillations, etc.

5 Conclusion and discussion

This paper aims to predict some possible dynamical behaviors of a flexible joint system by modeling the motions of an industrial robot manipulator. Some main conclusions are drawn as follows.

(1) The structure under consideration may be modeled to be a slow-fast delayed system when the moment of inertia of the lightweight link (or arm) is far less than that of the heavy rotor. The transformation delay from driving to acting arises from the flexible connection or joint between the rotor and the link. To model such a transformation delay, a delay in time scale is used.

(2) The geometric singular perturbation method can be extended to analyze the stability and the oscillations of a slow-fast system. Meanwhile, both the slow and the fast manifolds can be expressed analytically. The stability of the slow manifold is investigated and the critical boundaries are obtained, which bound the stable and the unstable regions. Stability analysis shows that a very small delay does not affect the stability of the slow manifold but a large delay does.

(3) The driving force, derived from the negative feedback of the link, determines the intersection of the slow and the fast manifolds. We have considered two quantitatively different driving forces to investigate the stability and the oscillations of the system under consideration. For the case of a small delay, both the link and the rotor exhibit stable state under the first kind of driving force but lose their stability and undergo relaxation oscillation under the second kind of driving force. For the case of a large delay, two types of driving forces lead to a regular periodic oscillation and a bursting oscillation, respectively. That is, the instability of the system becomes worse. It implies that an appropriate design for both the flexible joint and the driving force is of essential importance.

References

1 Zheng, Y.G., Wang, Z.H.: Advances in dynamics of slow-fast systems with time delay. Advances in Mechanics **41**, 400–410 (2011) (in Chinese)

2 Erzgräber, H., Lenstra, D., Krauskopf, B., et al.: Mutually delay-coupled semiconductor lasers: Mode bifurcation scenarios. Optics Communications **255**, 286–296 (2005)

3 Boudjellaba, H., Sari, T.: Dynamic transcritical bifurcations in a class of slow-fast predator-prey models. Journal of Differential Equations **246**, 2205–2225 (2009)

4 Fasano, A., Herrero, M.A., Rodrigo, M.R.: Slow and fast invasion waves in a model of acid-mediated tumour growth. Mathematical Biosciences **220**, 45–56 (2009)

5 Ji, Y., Bi, Q.S.: Bifurcation analysis of slow-fast behavior in modified Chua's circuit. Acta Physica Sinica **61**, 010202-1-010202-6 (2012)

6 Spong, M.W.: Modeling and control of elastic joint robots. Journal of Dynamic Systems, Measurement, and Control **109**, 310–319 (1987)

7 Fateh, M.M., Babaghasabha, R.: Impedance control of robots using voltage control strategy. Nonlinear Dynamics **74**, 277–286 (2013)

8 Consolini, L., Gerelli, O., Bianco, C.G.L., et al.: Flexible joint control: A minimum-time feed-forward technique. Mechatronics **19**, 348–356 (2009)

9 Ott, C., Albu-Schaffer, A., Kugi, A., et al.: On the passivity-based impedance control of flexible joint robots. IEEE Transactions on Robotics **24**, 416–429 (2008)

10 Brogardh, T.: Present and future robot control development—An industrial perspective. Annual Reviews in Control **31**, 69–79 (2007)

11 Marc, J.R., Li, C.: Controlling robot manipulators by dynamic programming. Acta Mechanica Sinica **11**, 20–33 (1995)

12 Subudhi, B., Morris, A.S.: Dynamic modeling, simulation and control of a manipulator with flexible links and joints. Robotics and Autonomous Systems **41**, 257–270 (2002)

13 Dwivedy, S.K., Eberhard, P.: Dynamic analysis of flexible manipulators, a literature review. A Mechanism and Machine Theory **41**, 749–777 (2006)

14 Chen, G.R., Shieh, L.S.: On trajectory tracking of time-delayed systems with an application to flexible-joint robot arm. In: Proceedings of International Conference on Control and Information, Chinese University Press, Hong Kong (1995)

15 Chen, G.R., Desages, A., Julian, P.: Trajectory tracking and robust stability for a class of time-delayed flexible joint. International Journal of Control **68**, 259–276 (1997)

16 Ailon, A.: Asymptotic stability in a flexible-joint robot with model uncertainty and multiple time delays in feedback. Journal of the Franklin Institute **341**, 519–531 (2004)

17 Valenzuela, M.A., Bentley, J.M., Lorenz, R.D.: Evaluation of torsional oscillations in paper machine sections. IEEE Transactions on Industry Applications **41**, 493–501 (2005)

18 Guckenheimer, J., Hoffman, K., Weckesserx, W.: Bifurcations of relaxation oscillations near folded saddles. International Journal of Bifurcation and Chaos **15**, 3411–3421 (2005)

19 Zheng, Y.G., Wang, Z.H.: Time-delay effect on the bursting of the synchronized state of coupled Hindmarsh-Rose neurons. Chaos **22**, 043127 (2012)

20 Lu, Q.S., Gu, H.G., Yang, Z.Q., et al.: Dynamics of firing patterns, synchronization and resonances in neuronal electrical activities: Experiments and analysis. Acta Mechanica Sinica **24**, 593–628 (2008)

21 Nayfeh, A.H.: Perturbation Methods. John Wiley & Sons, Inc, New York (1973)

22 Tikhonov, A.N.: Systems of differential equations containing a small parameter multiplying the derivative. Matematicheskii sbornik **31**, 575–586 (1952)

23 Fenichel, N.: Geometric singular perturbation theory for ordinary differential equations. Journal of Differential Equations **31**, 53–98 (1979)
24 Jones, C.: Geometric singular perturbation theory. Lecture Notes in Math **1609**, 45–118 (1994)
25 Rinaldi, S., Scheffer, M.: Geometric analysis of ecological models with slow and fast process. Ecosystems **3**, 507–521 (2000)
26 Izhikevich, E.M.: Neural excitability, spiking and bursting. International Journal of Bifurcation and Chaos **10**, 1171–1266 (2000)
27 Han, X., Jiang, B., Bi, Q.S.: Symmetric bursting of focus-focus type in the controlled Lorenz system with two time scales. Physics Letters A **373**, 3643–3649 (2009)
28 Ghorbel, F., Spong, M.W.: Integral manifolds of singularly perturbed systems with application to rigid-link flexible-joint multibody systems. International Journal of Non-Linear Mechanics **35**, 133–155 (2000)
29 Hori, Y., Iseki, H., Sugiura, K.: Basic consideration of vibration suppression and disturbance rejection control of multi-inertia system using SFLAC (State feedback and load acceleration control). IEEE Transactions on Industry Applications **30**, 889–896 (1994)
30 Nordin, M., Gutman, P.: Controlling mechanical systems with backlash-a survey. Automatica **38**, 1633–1649 (2002)
31 Naidu, D.S.: Singular perturbations and time scales in control theory and applications: An overview. Dynamics of Continuous, Discrete and Impulsive Systems Series B: Applications & Algorithms **9**, 233–278 (2002)
32 Xu, J., Chung, K.W., Chan, C.L.: An efficient method for studying weak resonant double hopf bifurcation in nonlinear systems with delayed feedbacks. SIAM J. Applied Mathematics **6**, 29–60 (2007)
33 Xu, J., Chung, K.W.: Effects of time delayed position feedback on a van der Pol-Duffing oscillator. Physica D **180**, 17–39 (2003)
34 Wang, L.L.: Foundation of Stress Waves. (2nd edn.) National Defense Industry Press, Beijing (2005) (in Chinese)
35 Xu, J., Lu, Q.S., Huang, K.L.: Controlling erosion of safe basin in nonlinear parametrically excited systems. Acta Mechanica Sinica **12**, 281–288 (1996)
36 Wang, W.Y., Pei, L.J.: Stability and Hopf bifurcation of a delayed ratio-dependent predator-prey system. Acta Mechanica Sinica **27**, 285–296 (2011)
37 Wang, H.L., Wang, Z.H., Hu, H.Y.: Hopf bifurcation of an oscillator with quadratic and cubic nonlinearities and with delayed velocity feedback. Acta Mechanica Sinica **20**, 426–434 (2004)
38 Zhang, S., Xu, J.: Bursting-like motion induced by time-varying delay in an internet congestion control model. Acta Mechanica Sinica **28**, 1169–1179 (2012)